Covalently interconnected transition metal dichalcogenide networks *via* defect engineering for high-performance electronic devices

Stefano Ippolito[a], Adam G. Kelly[b], Rafael Furlan de Oliveira[a], Marc-Antoine Stoeckel[a], Daniel Iglesias[a], Ahin Roy[c], Clive Downing[c], Zan Bian[d], Lucia Lombardi[d], Yarjan Abdul Samad[d], Valeria Nicolosi[c], Andrea C. Ferrari[d], Jonathan N. Coleman[b], Paolo Samorì[a,*]

[a] Université de Strasbourg, CNRS, ISIS UMR 7006, 8 allée Gaspard Monge, F-67000 Strasbourg, France
[b] School of Physics, Centre for Research on Adaptive Nanostructures and Nanodevices (CRANN) and Advanced Materials and Bioengineering Research (AMBER), Trinity College Dublin, Dublin 2, Ireland
[c] School of Chemistry, Centre for Research on Adaptive Nanostructures and Nanodevices (CRANN) and Advanced Materials and Bioengineering Research (AMBER), Trinity College Dublin, Dublin 2, Ireland
[d] Cambridge Graphene Centre, Cambridge University, 9 JJ Thomson Avenue, Cambridge CB3 OFA, United Kingdom

* Corresponding author: samori@unistra.fr

Solution-processed semiconducting transition metal dichalcogenides (TMDs) are at the centre of an ever-increasing research effort in printed (opto)electronics. However, device performance is limited by structural defects resulting from the exfoliation process and poor inter-flake electronic connectivity. Here, we report a new molecular strategy to boost the electrical performance of TMD-based devices *via* the use of dithiolated conjugated molecules, to simultaneously heal sulfur vacancies in solution-processed transition metal disulfides (MS_2) and covalently bridge adjacent flakes, thereby promoting percolation pathways for the charge transport. We achieve a reproducible increase by one order-of-magnitude in field-effect mobility (μ_{FE}), current ratios (I_{ON}/I_{OFF}), and switching times (τ_S) of liquid-gated transistors, reaching 10^{-2} $cm^2 V^{-1} s^{-1}$, 10^4, and 18 ms, respectively. Our functionalization strategy is an universal route to simultaneously enhance the electronic connectivity in MS_2 networks and tailor *on demand* their physicochemical properties according to the envisioned applications.

Solution-processed layered materials have a wide-ranging portfolio of physicochemical properties, whose inherent features make them prime candidates for low-cost and scalable applications in (opto)electronics, (photo)catalysis, (bio)sensing, and biomedicine[1,2,3,4]. Much work has been done on the production and isolation of solution-processed semiconducting transition metal dichalcogenides (TMDs) by scalable methods[5,6,7]. Liquid-phase exfoliation (LPE) is the main route to attain high concentration and high volume TMD dispersions[8,9], where bulk crystals are dispersed and exfoliated in a specific solvent *via* a mechanical energy transfer that overcomes the Van der Waals interactions within the layered structures. The high throughput achieved by LPE promotes the use of TMDs in many different applications, exploiting pristine or hybrid materials in the form of dispersions, coatings, and thin-films produced by diverse deposition techniques including inkjet printing, spray coating, roll-to-roll, drop-casting, etc[10,4,11,7].

Although LPE provides the best trade-off amongst cost, purity, yield, etc.[12,11], it has some limitations when the final application concerns (opto-)electronics, where structural defects in the materials play a detrimental role[1,13]. One of the most widely employed LPE methods makes use of a tip horn sonicator that peels layered materials apart, thanks to vibrational and cavitation forces that arise from the generation and propagation of transverse waves within the solvent[14]. Consequently, the formation and implosion of cavitation bubbles generates energetic shock waves that induce local temperature and pressure conditions sufficient to peel individual layers off the bulk structure, with critical influence on their ultimate lateral size[15]. This energetic exfoliation procedure results in a mild formation of new defects, as well as major propagation of inherent bulk defects in the exfoliated layers. Supported by thermodynamic considerations, zero-dimensional defects are the most abundant stoichiometric deficiencies in TMDs, especially chalcogen vacancies that are mainly located at the flake edges and whose formation energy is a few eV (~2 eV in the case of sulfur vacancies)[16,17]. These structural defects strongly affect the electronic properties of solution-processed TMDs, with detrimental effects on the electrical performance of related devices[18,19].

Many groups developed molecular strategies to tune the physicochemical properties of solution-processed TMDs and overcome the aforementioned limitations, enlarging their range of applicability in electronics and optoelectronics[20,21,22]. In the case of electronic applications based on individual

flakes, a promising strategy exploits thiolated molecular systems to heal sulfur vacancies (V_S) in transition metal disulfides (MS_2), thereby restoring the material pristine crystal structure and enhancing its electrical properties[23,24]. Nevertheless, in thin-film TMD-based devices, an additional and limiting factor related to the inter-flake electrical resistance emerges, resulting in a significant hindrance of charge carrier transport[25,26]. This represents a major bottleneck in the development of solution-processed TMD-based optoelectronics, especially in large-area and high-performance device applications.

Here, we report a molecular strategy to simultaneously heal V_S in solution-processed MS_2 (M = Mo, W, and Re) and increase the inter-flake electronic connectivity by means of dithiolated molecular systems. Using π-conjugated dithiolated molecules (HS-R-SH), we prove *via* diverse multiscale analysis the simultaneous: i) healing of V_S to restore the MS_2 crystal structure and decrease the related stoichiometric deficiencies acting as charge scattering centres, ii) the covalent bridging of adjacent flakes, resulting in an enhanced charge carrier transport through an interconnected network. We investigate and capitalize on the *in-situ* functionalization approach of TMDs, exposing the inorganic materials to molecular linkers just after their deposition on a substrate. This is crucial for the formation of long-range pathways which exhibit superior charge transport characteristics, likewise the bridging of disordered regions in conjugated polymer chains[27].

Such an approach represents an innovative and universal functionalization method capable of improving the performance of devices based on solution-processed MS_2 for large-area electronic applications. We apply this strategy in liquid-gated thin-film transistors (LG-TFTs) fabricated by drop-casting MS_2 dispersions onto SiO_2/Si substrates pre-patterned with interdigitated gold electrodes (IDEs), followed by exposure to aromatic and conjugated 1,4-benzenedithiol (BDT) molecules. This boosts the characteristics of MS_2-based LG-TFTs by one order-of-magnitude, leading to state-of-the-art electrical performance characterized by competing field-effect mobilities (μ_{FE}) and I_{ON} / I_{OFF}, along with the fastest switching speed reported to date for devices of this kind[28]. Improved water stability and mechanical robustness are other unique features exhibited by the covalently bridged MS_2 networks.

Device fabrication and *in-situ* functionalization.

MS_2 colloidal dispersions (inks), with M = Mo, W and Re, are produced and characterized prior to their use in devices (see Supplementary Sections 1 and 2). MS_2 inks are then drop-cast onto SiO_2/Si substrates with 2.5 μm-spaced Au IDEs for TFT measurements. The ink deposition is performed on the substrate placed onto a 110°C heated hot plate to assist the solvent (2-propanol) evaporation and the elimination of humidity traces during casting (Fig. 1a). Morphological characterizations (SEM and AFM) of the deposited materials show a large(μm)-scale uniform coverage of the electrodes (important to enable charge percolation pathways), thickness = 700 ± 100 nm, and average root-mean-square roughness R_{rms} = 95 ± 10 nm over a 25 μm^2 area (Supplementary Fig. 3a).

In our work, MS_2 networks are formed by bridging adjacent flakes and taking advantage of the higher defect density at the edge sites with respect to basal planes, as confirmed by high-angle annular dark-field scanning transmission electron microscopy investigation (STEM) (Supplementary Fig. 2). More specifically, the MS_2 thin films are functionalized in a N_2-filled glovebox exploiting a 50 mM saturated solution of BDT in anhydrous hexane to promote the formation of a covalently-linked MS_2 networks. The whole BDT solution preparation (powder weighing and dissolution) is carried out under N_2-controlled atmosphere to avoid thiol oxidation reactions induced by impurities[29]. The coated slides are soaked in BDT solution at room temperature for 24 h inside a sealed container, followed by rinsing in hexane, and annealing onto a hot plate at 90°C for 30 min. No significant morphological variations are detected after thiol exposure, and the network features remain similar to those of the pristine films (Supplementary Fig. 3b). The functionalization process is designed to simultaneously heal V_S in MS_2 films and covalently bridge adjacent flakes, thereby promoting their modification at the molecular level (Fig. 1b).

Multiscale characterization of MS_2 networks.

We assess the effects of *in-situ* functionalization with BDT molecules by independent multiscale techniques. XPS measurements provide evidence for MS_2 chemical functionalization, as illustrated in Fig. 2a by the S2p high-resolution spectra of drop-cast solution-processed molybdenum disulfide (MoS_2) before (as film) and after (as network) BDT treatment. The MoS_2 S2p spectrum displays two

main peaks at ~162.3 and ~163.5 eV, assigned to the $S2p_{3/2}$ and $S2p_{1/2}$ components[30], respectively. An additional component can be deconvoluted at ~161.5 eV and ascribed to defects, *e.g.* vacancy neighbouring S atoms[30,31]. Such a minority component at lower binding energies is due to the charge localized on S, that, once S is desorbed, can be redistributed on the first neighbouring atoms, enhancing Coulomb screening[30]. The substroichiometric MoS_{2-x} component at ~161.5 eV is related to unsaturated S ligands[31], such as V_S, and decreases from 8.0 ± 0.5 % to 5.0 ± 0.5 % upon BDT treatment, proving how the exposure to thiolated molecules leads to a decrease of chalcogen vacancy defects in solution-processed MoS_2. Since different S ligands have minimal differences in binding energies, their identification in XPS spectra is not always straightforward, and most literature focuses just on MoS_2 (see Supplementary Section 4 for further information on XPS data analysis).

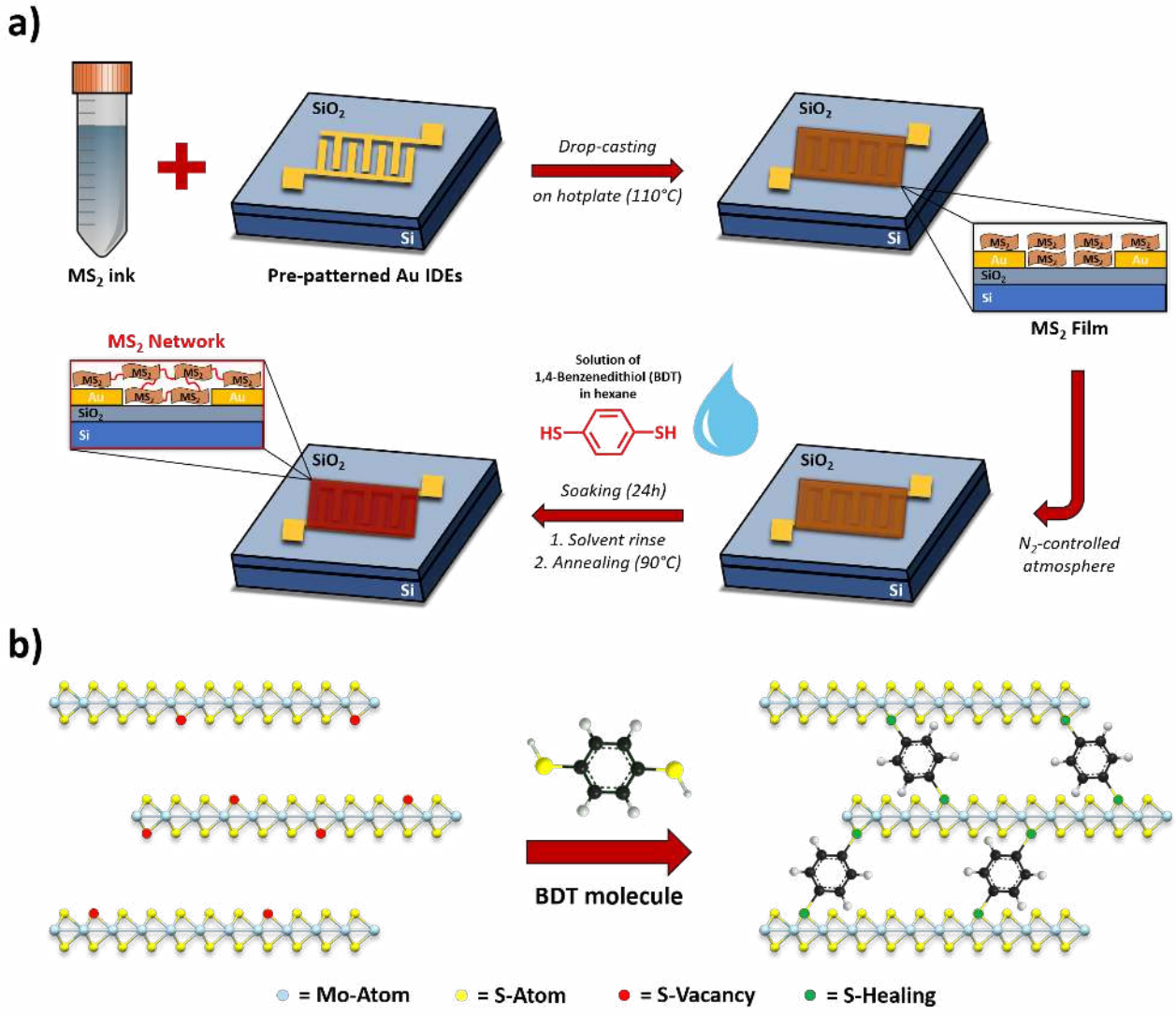

Figure 1 | Functionalization strategy to produce covalently interconnected MS_2 networks. a, illustration of ink deposition and *in-situ* functionalization to produce MS_2 networks *via* BDT treatment. **b**, Sketch of V_S healing mechanism in MoS_2 films by means of dithiolated molecules and related inter-flake networking.

Raman spectra of MoS_2 pristine films and networks (Fig. 2b) show no major differences, suggesting that the functionalization process does not damage the flakes. The full width at half maximum (FWHM) of both E^1_{2g} and A_{1g} peaks shows a narrowing of ~ 10% upon thiol exposure, as well as small blue shift and increase of the E^1_{2g} / A_{1g} intensity ratio (see Supplementary Section 5). This is consistent with a reduction in defect density and suppression of defect-activated modes[32,33], endorsing the healing of V_S by thiolated molecules. An extended and rigorous statistical Raman analysis of MoS_2 films and networks is provided in Supplementary Section 5.

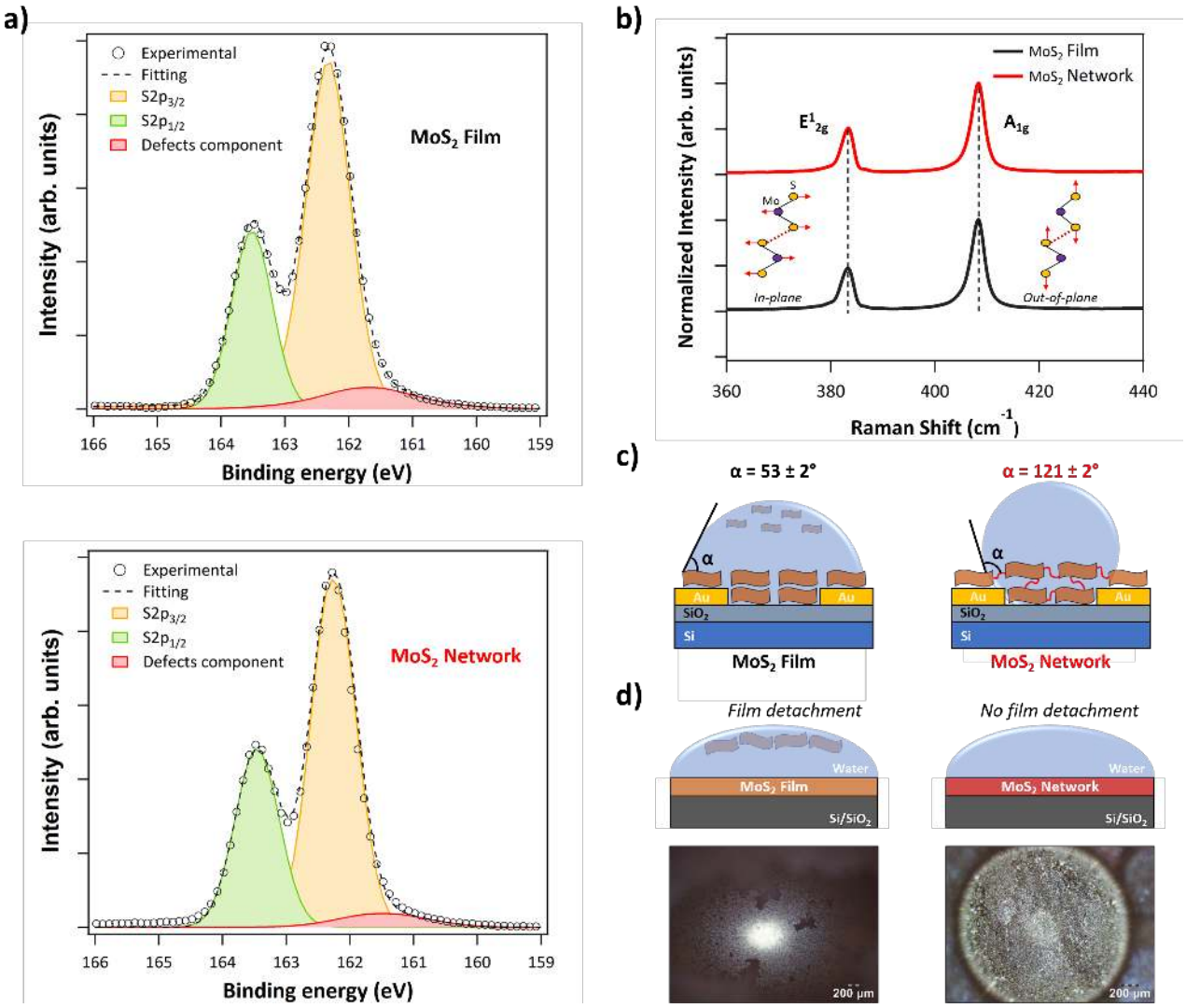

Figure 2 | Characterization of MS_2 films and networks. a, High-resolution S2p XPS spectra for MoS_2 films (top) and networks (bottom). **b**, Raman spectra of MoS_2 films (black) and networks (red), highlighting the two main E^1_{2g} and A_{1g} peaks related to in-plane and out-of-plane vibrations, respectively. **c**, Sketch of water contact angle results for MoS_2 films (left) and networks (right). **d**, Schematics (top) and optical images (bottom) showing the different water stability for MoS_2 films (left) and networks (right).

An evidence of the network formation comes from the distinctive characteristics and macroscopic properties of BDT-treated MS_2 samples. Pristine MoS_2 films on electrode-free SiO_2/Si substrates exhibit a hydrophilic behaviour, with an average static water contact angle (WCA) of 53 ± 2° in agreement with literature[34], whereas small fluctuations around these numbers depend on material growth, exfoliation, and deposition techniques[35]. Upon functionalization, the MoS_2 networks show a strong hydrophobic behaviour characterized by an average WCA of 121 ± 2° (Fig. 2c), where the free aromatic and non-polar ring of BDT molecules remain exposed to the samples' surface increasing its hydrophobicity (see Supplementary Section 6). The network formation in BDT-functionalized MoS_2 samples improves the material stability in water (Fig. 2d and Supplementary Fig. 12). For MoS_2 pristine films we observe detachment and floating of the material exposed to water, while for MoS_2 networks the sample integrity is preserved. The solvation process is hindered within the MoS_2 network (less soluble than isolated free single flakes), consistent with the covalent interconnectivity promoted by dithiolated linkers. Such a feature is of primary importance for the fabrication of robust devices operating in aqueous environment[2]. An additional evidence of network formation comes from the *ex-situ* functionalization of MoS_2 flakes in solution[36,37], where the bridging process induced by BDT linkers compromises the colloidal stability and undermines the electrical performance of the corresponding LG-TFTs (see Supplementary Section 9)[38,39]. All the above-mentioned features of the networks cannot be achieved by using monothiolated functionalizing molecules (thiophenol, TP), that are unlikely to bridge adjacent flakes (see Supplementary Section 6). Improved mechanical robustness was observed in MS_2 networks deposited onto flexible substrates and subjected to multiple (5-10k) deformations, highlighting another advantageous effect of the covalent bridging (see Supplementary Section 6, Supplementary Fig. 13).

LG-TFTs based on MS_2 films and networks.

The covalent bridging of individual MS_2 flakes with π-conjugated molecules is expected to improve the material's electrical properties, especially its electrical connectivity, where long-range electronic delocalization is advocated[27]. We thus investigate the performance of TFTs based on pristine MoS_2 films and networks. Dielectrically-gated TFTs based on solution-processed TMDs show poor current switching ($I_{ON} / I_{OFF} < 10$)[40], encouraging one to focus on TFTs where the semiconductor layer is electrolytically gated by means of an ionic liquid (IL) solution (Fig. 3a), exploiting the inherent disorder and related porosity of the deposited materials. For LG-TFTs based on solution-processed TMD flakes, the liquid dielectric penetrates the internal free volume of the semiconducting material, thus gating the device volumetrically[28].

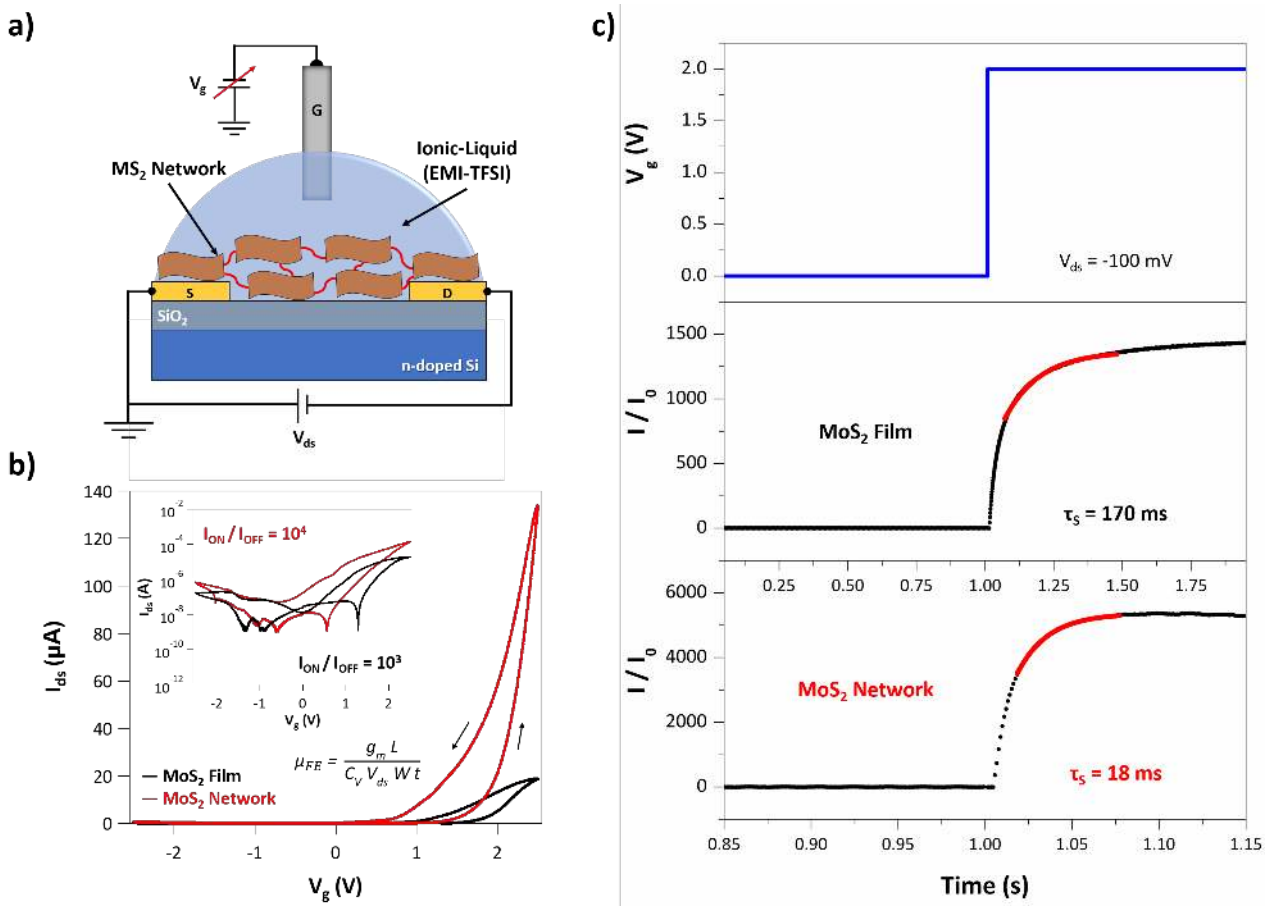

Figure 3 | Electrical properties of LG-TFTs based on MoS_2 films and networks. a, LG-TFT geometry. **b**, Transfer curves for MoS_2 films and networks with V_{ds} = -100 mV and V_g sweeping from -2.5 V to +2.5 V. *Inset:* log-scale current characteristics and equation to calculate μ_{FE}. **c**, LG-TFT switching characteristics under V_g

step and corresponding time-dependent normalized current response (I / I_0). The red line delimits the range in which a non-linear fitting can be used to extrapolate τ_S.

All our LG-TFT measurements are performed under N_2-controlled glovebox atmosphere, to avoid side effects of environmental adsorbates, such as water and oxygen, that can induce strong p-doping[41]. Fig. 3b displays the transfer curves (I_{ds} *vs*. V_g) of LG-TFTs based on MoS_2 films and networks. Both show n-type transfer characteristics, with the latter featuring an overall superior performance. In particular, MoS_2 networks exhibit higher μ_{FE} up to 10^{-2} cm^2 V^{-1} s^{-1} and I_{ON} / I_{OFF} ratios up to 10^4, one order-of-magnitude greater than pristine MoS_2 films (see Supplementary Section 7 for the calculation of the device figures of merit and related statistical analysis). No significant differences in threshold voltage (V_{TH}) are observed upon bridging of flakes, proving that BDT linkers mainly affect the conductivity of the networks in terms of μ_{FE} and not the charge carrier density (doping effect)[42].

Likewise, a similar outcome is observed for the switching time (τ_S) of LG-TFTs based on MoS_2 films and networks, while applying a step-like V_g stimulus and measuring the device time-dependent current response. Here, τ_S is ~170 ms for MoS_2 films and ~18 ms for the networks (Fig. 3c), meaning that covalently interconnected systems result in one order-of-magnitude faster devices, with state-of-the-art switching performance for transistors of this kind[28]. The electrical characteristics and LG-TFT figures of merit of other solution-processed TMDs are in the Supplementary Section 7. The reproducible 10-fold enhancement of device performance observed for MS_2 networks supports the considerations envisaged for interconnected systems by π-conjugated and dithiolated linkers (Table 1), unachievable for monothiolated TP molecules, that do not allow network formation (Supplementary Fig. 20). The bridging process of adjacent flakes attained with aliphatic dithiolated molecules barely improves the electrical characteristics of MoS_2 LG-TFTs, whose performance cannot rival those achieved with BDT π-conjugated linkers (Supplementary Fig. 22).

Temperature-dependent electrical characteristics.

MoS_2 films and networks have also been analysed by measuring their current *vs*. electric field (I-E) characteristics as a function of temperature (T) in high vacuum (10^{-6} Torr). The samples are prepared

on SiO_2/Si substrates with Au IDEs. The average field E is calculated from V = E x *d*, where V is the applied bias voltage and *d* is the IDE channel distance (2.5 μm). I-E relations are used with equations describing charge transport models[43]. The charge transport characteristics are measured with and without a back-gate voltage (V_G^{Back}) on the n^{++}-Si substrate. At room temperature, and with V_G^{Back} = 0, minor differences are found between the I-E traces of MoS_2 films and networks (Fig. 4a). For T ranging from 250 to 300 K, the current characteristics indicate Schottky emission as the dominant charge transport mechanism (Fig. 4b). The formation of a Schottky barrier (Fig. 4b inset) with height Φ_B at the metal/MoS_2 interface was previously investigated[44]. From the thermionic emission formalism (Equation S4)[43], we estimate the Au/MoS_2 Φ_B = 366 ± 1 meV for MoS_2 pristine films, Φ_B = 285 ± 7 meV for MoS_2 networks, and Φ_B = 288 ± 16 meV for TP-functionalized MoS_2 (Supplementary Fig. 24-25). Such a reduction of Φ_B upon both thiol functionalization (BDT and TP) points to either a modification of the Au work-function (Φ_{WF}) and/or healing of Au/MoS_2 interface states[45]. Measurements of Φ_{WF} for Au electrode surfaces by PhotoElectron Spectroscopy in Air (PESA), before and after thiol treatment, reveal a small decrease from 5.11 ± 0.02 eV (bare Au) to 4.97 ± 0.10 eV and 4.93 ± 0.07 eV for BDT and TP, respectively (Table S6). Such a small Φ_{WF} change is consistent with the passivation of Au/MoS_2 interfaces states — due to the healing of V_S in the material — as the main cause of Φ_B reduction in thiol functionalized samples[45]. Such a small Φ_{WF} reduction, as well as similar values found for BDT and TP-functionalized samples, cannot explain the enhanced device performance exhibited by MoS_2 networks in LG-TFTs.

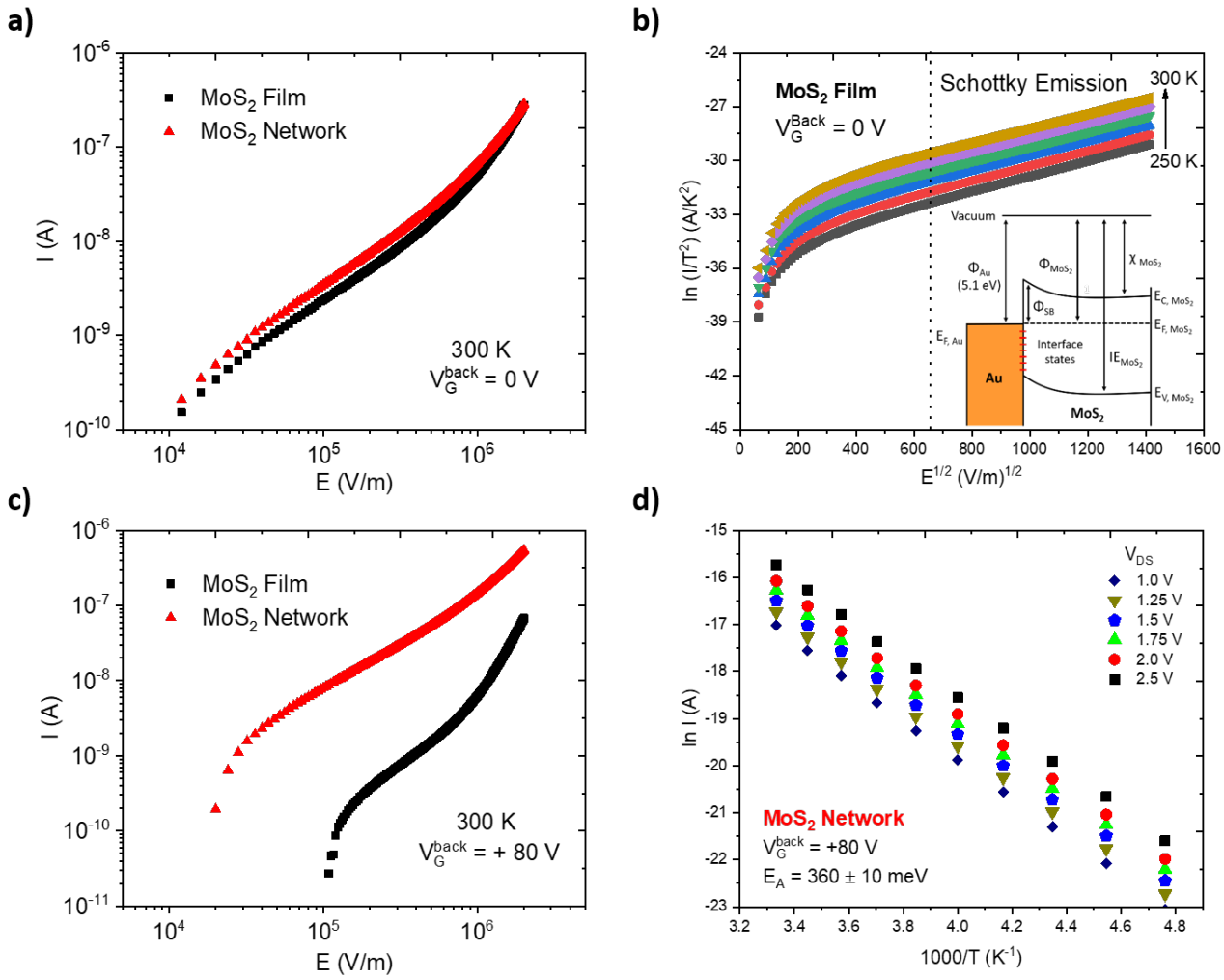

Figure 4 | Temperature-dependent electrical characteristics. a, 300K I-E curves for V_G^{Back} = 0 for MoS_2 films (black) and networks (red). **b**, Schottky plot for MoS_2 film for V_G^{Back} = 0 V. *Inset*: Band diagram for Au/MoS_2 Schottky barrier interface. **c**, 300K I-E characteristic with for V_G^{Back} = +80 V in MoS_2 films (black) and networks (red). **d**, Arrhenius plot for MoS_2 network for V_G^{Back} = +80 V.

As for LG-TFTs (Fig. 3), the superior electrical performance of MoS_2 networks arise when the Schottky barrier is attenuated by the application of a V_G[46]. Fig. 4c plots the room-temperature I-E characteristics of samples under high V_G^{Back} = +80 V. A ~10-fold current difference is observed for MoS_2 networks when compared to films, especially at intermediate fields (E= 10^5-10^6 V/m), a condition that mimics the LG-TFT operating parameters (E ~10^5 V/m). For T = 250-300 K and E = 1 MV/m, MoS_2 films and networks have a thermally-activated current response (Fig. 4d and Supplementary Fig. 26) with significantly different activation energies (E_A), *i.e.* 512 ± 12 meV and 360 ± 10 meV, respectively. E_A of hundreds of meV reflect the energy necessary to overcome the inter-flake barriers in MoS_2 systems[26], rather than low-energy (tens of meV) intra-flake conduction

states[26]. By sweeping V_G^{Back} from -60 to +60 V, the T-dependent charge carrier mobility μ(T) of films and networks follows an Arrhenius relation, with lower E_A for networks (Supplementary Fig. 27). Hence, as inter-flake processes appear to be the limiting factor for charge transport within TMD thin-films[41], a reduced E_A points out an improved bulk connectivity among adjacent flakes (network formation). E_A for TP-functionalized samples (500 ± 1 meV) are only slightly smaller than the values found for pristine MoS_2 films, revealing a reduction of trap states caused by the V_S healing mechanism, without any further improvement due to the inter-flake connectivity (see Supplementary Section 8).

Conclusions

We reported a universal and simple route to produce covalently interconnected TMD networks by exploiting defect engineering in solution-processed layered materials. We used π-conjugated dithiolated molecules to bridge adjacent MS_2 flakes, forming networks characterized by substantially different physicochemical properties (improved electrical characteristics, water stability, and mechanical robustness). The bridging of neighbouring flakes at the molecular level improves the charge transport across the network, thereby leading to superior device performances. LG-TFTs show a reproducible one order-of-magnitude increase in the main figures of merit, leading to state-of-the-art field-effect mobility (10^{-2} cm^2 V^{-1} s^{-1}) and I_{ON} / I_{OFF} ratio (10^4), along with the fastest switching time (18 ms) reported for devices of this kind[28,47]. Our findings pave the way for the development of high-performance, large-area and printed electronics based on solution-processed TMDs. The network formation results in water-stable and mechanically robust MS_2-based devices, that could be exploited in (bio)sensing[48], (photo)catalisyis[2], and flexible optoelectronics[49]. Ultimately, with an appropriate molecular design of the bridging linkers, one might endow the TMD networks with diverse functionalities, tuning the final properties *on demand* according to the final applications.

Figure of Merit	**MoS_2 Film**	**MoS_2 Network**
$\mu_{FE} / \mu_{FE,\ film}$	**1**	**10 ± 1**
I_{ON} / I_{OFF}	**10^3**	**10^4**
V_{TH}	**(1.9 ± 0.1) V**	**(1.8 ± 0.1) V**
τ_S	**(170 ± 5) ms**	**(18 ± 2) ms**

Table 1 | Main figures of merit for MoS_2 film and network-based electrical devices. Upon exposure to BDT and network formation, LG-TFTs exhibit a reproducible one order-of-magnitude enhancement in the main device figures of merit, with minimal changes in V_{TH}.

Methods

Device preparation. Bottom-contact SiO_2 / n^{++}-Si substrates (15 mm x 15 mm, Fraunhofer IPMS, Dresden, Germany) are used. The substrates consist of thermally grown SiO_2 (230 nm thick) having IDEs (30 nm thick Au onto 10 nm ITO adhesion layer) spaced 2.5 µm, yielding a channel width-length (W/L) ratio ~4000. Prior to use, the substrates are cleaned by ultrasonication in acetone and 2-propanol (10 min each), and dried under N_2 flow afterwards.

The films are moved in a N_2-filled glovebox for the following functionalization steps: i) sample immersion in a 50 mM saturated solution BDT in anhydrous hexane for 24 h inside a sealed container, ii) spin-rinsing with anhydrous hexane (5 ml, 4000 rpm, acceleration 4000 rpm s^{-1}, 60 s) and iii) annealing at 90°C for 30-45 min.

Electrical characterization. The LG-TFT performances are evaluated by their transfer characteristics (I_{ds} *vs*. V_g), using a Pt wire as the gate electrode and a droplet of 1-ethyl-3-methylimidazolium bis(trifluoromethylsulfonyl) imide EMI-TFSI as IL gate dielectric. The source-drain current (I_{ds}) is recorded while sweeping gate voltage (V_g) from -2.5 to +2.5 V, at source-drain voltage V_{ds} = -0.1 V. The current-electric field traces (I_{ds} - E) are measured for T = 80-300K, in an Oxford Instruments Optistat DN-V cryostat, for V_G^{Back} = 0 and +80 V. All electrical measurements are carried out in dark and under N_2-controlled atmosphere using a Keithley 2636A SourceMeter unit. In order to rely on a strong statistical analysis, nearly 60 identical devices were produced and subjected to the different electrical characterizations.

Further details about the materials, characterization techniques and data treatment can be found in the Supplementary Information file.

Data availability

The data that support the findings of this study are available from the corresponding author upon reasonable request.

References

1. Wang, Q. H., Kalantar-Zadeh, K., Kis, A., Coleman, J. N. & Strano, M. S. Electronics and optoelectronics of two-dimensional transition metal dichalcogenides. *Nat. Nanotechnol.* **7**, 699–712 (2012).
2. Voiry, D., Yang, J. & Chhowalla, M. Recent strategies for improving the catalytic activity of 2D TMD nanosheets toward the hydrogen evolution reaction. *Adv. Mater.* **28**, 6197–6206 (2016).
3. Chen, Y., Tan, C., Zhang, H. & Wang, L. Two-dimensional graphene analogues for biomedical applications. *Chem. Soc. Rev.* **44**, 2681–2701 (2015).
4. Ferrari, A. C. *et al.* Science and technology roadmap for graphene, related two-dimensional crystals, and hybrid systems. *Nanoscale* **7**, 4598–4810 (2015).
5. Manzeli, S., Ovchinnikov, D., Pasquier, D., Yazyev, O. V. & Kis, A. 2D transition metal dichalcogenides. *Nat. Rev. Mater.* **2**, 1–15 (2017).
6. Han, J. H., Kwak, M., Kim, Y. & Cheon, J. Recent advances in the solution-based preparation of two-dimensional layered transition metal chalcogenide nanostructures. *Chem. Rev.* **118**, 6151–6188 (2018).
7. Backes, C. *et al.* Production and processing of graphene and related materials. *2D Mater.* **7**, 022001 (2020).
8. O'Neill, A., Khan, U. & Coleman, J. N. Preparation of high concentration dispersions of exfoliated MoS_2 with increased flake size. *Chem. Mater.* **24**, 2414–2421 (2012).
9. Yao, Y. *et al.* High-concentration aqueous dispersions of MoS_2. *Adv. Funct. Mater.* **23**, 3577–3583 (2013).
10. Bonaccorso, F., Bartolotta, A., Coleman, J. N. & Backes, C. 2D-Crystal-based functional inks. *Adv. Mater.* **28**, 6136–6166 (2016).
11. Bonaccorso, F. *et al.* Production and processing of graphene and 2d crystals. *Materials Today* **15**, 564–589 (2012).
12. Raccichini, R., Varzi, A., Passerini, S. & Scrosati, B. The role of graphene for electrochemical energy storage. *Nat. Mater.* **14**, 271–279 (2015).
13. Jariwala, D., Sangwan, V. K., Lauhon, L. J., Marks, T. J. & Hersam, M. C. Emerging device applications for semiconducting two-dimensional transition metal dichalcogenides. *ACS Nano* **8**, 1102–1120 (2014).
14. Ciesielski, A. & Samorì, P. Graphene via sonication assisted liquid-phase exfoliation. *Chem. Soc. Rev.* **43**, 381–398 (2014).
15. Backes, C. *et al.* Equipartition of energy defines the size–thickness relationship in liquid-exfoliated nanosheets. *ACS Nano* **13**, 7050–7061 (2019).

16. Tsai, C. *et al.* Electrochemical generation of sulfur vacancies in the basal plane of MoS_2 for hydrogen evolution. *Nat. Commun.* **8**, 15113 (2017).
17. Komsa, H.-P. *et al.* Two-dimensional transition metal dichalcogenides under electron irradiation: defect production and doping. *Phys. Rev. Lett.* **109**, 035503 (2012).
18. McDonnell, S., Addou, R., Buie, C., Wallace, R. M. & Hinkle, C. L. Defect-dominated doping and contact resistance in MoS_2. *ACS Nano* **8**, 2880–2888 (2014).
19. Nicolosi, V., Chhowalla, M., Kanatzidis, M. G., Strano, M. S. & Coleman, J. N. Liquid exfoliation of layered materials. *Science* **340**, (2013).
20. Voiry, D. *et al.* Covalent functionalization of monolayered transition metal dichalcogenides by phase engineering. *Nat. Chem.* **7**, 45–49 (2015).
21. Ippolito, S., Ciesielski, A. & Samorì, P. Tailoring the physicochemical properties of solution-processed transition metal dichalcogenides via molecular approaches. *Chem. Commun.* **55**, 8900–8914 (2019).
22. Bertolazzi, S., Gobbi, M., Zhao, Y., Backes, C. & Samorì, P. Molecular chemistry approaches for tuning the properties of two-dimensional transition metal dichalcogenides. *Chem. Soc. Rev.* **47**, 6845–6888 (2018).
23. Schmidt, H., Giustiniano, F. & Eda, G. Electronic transport properties of transition metal dichalcogenide field-effect devices: surface and interface effects. *Chem. Soc. Rev.* **44**, 7715–7736 (2015).
24. Sim, D. M. *et al.* Controlled doping of vacancy-containing few-layer MoS_2 via highly stable thiol-based molecular chemisorption. *ACS Nano* **9**, 12115–12123 (2015).
25. Yu, X., Prévot, M. S. & Sivula, K. Multiflake thin film electronic devices of solution processed 2D MoS_2 enabled by sonopolymer assisted exfoliation and surface modification. *Chem. Mater.* **26**, 5892–5899 (2014).
26. Zeng, X., Hirwa, H., Metel, S., Nicolosi, V. & Wagner, V. Solution processed thin film transistor from liquid phase exfoliated MoS_2 flakes. *Solid-State Electron.* **141**, 58–64 (2018).
27. Noriega, R. *et al.* A general relationship between disorder, aggregation and charge transport in conjugated polymers. *Nat. Mater.* **12**, 1038–1044 (2013).
28. Kelly, A. G. *et al.* All-printed thin-film transistors from networks of liquid-exfoliated nanosheets. *Science* **356**, 69–73 (2017).
29. Schilter, D. Thiol oxidation: a slippery slope. *Nat. Rev. Chem.* **1**, 1–1 (2017).
30. Donarelli, M., Bisti, F., Perrozzi, F. & Ottaviano, L. Tunable sulfur desorption in exfoliated MoS_2 by means of thermal annealing in ultra-high vacuum. *Chem. Phys. Lett.* **588**, 198–202 (2013).

31. McIntyre, N. S., Spevack, P. A., Beamson, G. & Briggs, D. Effects of argon ion bombardment on basal plane and polycrystalline MoS_2. *Surf. Sci.* **237**, L390–L397 (1990).
32. Mignuzzi, S. *et al.* Effect of disorder on Raman scattering of single-layer MoS_2. *Phys. Rev. B* **91**, 195411 (2015).
33. Bae, S. *et al.* Defect-induced vibration modes of Ar^+-Irradiated MoS_2. *Phys. Rev. Applied* **7**, 024001 (2017).
34. Park, S. Y. *et al.* Highly selective and sensitive chemoresistive humidity sensors based on rGO/MoS_2 van der Waals composites. *J. Mater. Chem. A* **6**, 5016–5024 (2018).
35. Chow, P. K. *et al.* Wetting of mono and few-layered WS_2 and MoS_2 films supported on Si/SiO_2 Substrates. *ACS Nano* **9**, 3023–3031 (2015).
36. Nguyen, E. P. *et al.* Electronic tuning of 2D MoS_2 through surface functionalization. *Adv. Mater.* **27**, 6225–6229 (2015).
37. Chou, S. S. *et al.* Ligand conjugation of chemically exfoliated MoS_2. *J. Am. Chem. Soc.* **135**, 4584–4587 (2013).
38. Kim, J. *et al.* Direct exfoliation and dispersion of two-dimensional materials in pure water via temperature control. *Nat. Commun.* **6**, 1–9 (2015).
39. Graetzel, M., Janssen, R. A. J., Mitzi, D. B. & Sargent, E. H. Materials interface engineering for solution-processed photovoltaics. *Nature* **488**, 304–312 (2012).
40. Li, J., Naiini, M. M., Vaziri, S., Lemme, M. C. & Östling, M. Inkjet printing of MoS_2. *Adv. Funct. Mater.* **24**, 6524–6531 (2014).
41. Li, S.-L., Tsukagoshi, K., Orgiu, E. & Samorì, P. Charge transport and mobility engineering in two-dimensional transition metal chalcogenide semiconductors. *Chem. Soc. Rev.* **45**, 118–151 (2015).
42. Wang, Y., Gali, S. M., Slassi, A., Beljonne, D. & Samorì, P. Collective dipole-dominated doping of monolayer MoS_2: orientation and magnitude control via the supramolecular approach. *Adv. Funct. Mater.* **30**, 2002846 (2020).
43. Chiu, F.-C. A Review on conduction mechanisms in dielectric films. *Adv. Mater. Sci. Eng.* **2014**, 1–18 (2014).
44. Lee, K. *et al.* Electrical characteristics of molybdenum disulfide flakes produced by liquid exfoliation. *Adv. Mater.* **23**, 4178–4182 (2011).
45. Sze, S. M. & Ng, K. K. Physics of semiconductor devices. *John Wiley & Sons* (2006).
46. Vladimirov, I. *et al.* Bulk transport and contact limitation of MoS_2 multilayer flake transistors untangled via temperature-dependent transport measurements. *Phys. Status Solidi A* **212**, 2059–2067 (2015).

47. Higgins, T. M. *et al.* Electrolyte-gated n-type transistors produced from aqueous inks of WS_2 Nanosheets. *Adv. Funct. Mater.* **29**, 1804387 (2019).
48. Anichini, C. *et al.* Chemical sensing with 2D materials. *Chem. Soc. Rev.* **47**, 4860–4908 (2018).
49. Akinwande, D., Petrone, N. & Hone, J. Two-dimensional flexible nanoelectronics. *Nat. Commun.* **5**, 5678 (2014).

Acknowledgements

We acknowledge funding from European Commission through the Graphene Flagship, the ERC Grants SUPRA2DMAT (GA-833707), FUTURE-PRINT (GA-694101), Hetero2D, GSYNCOR, the EU Grant Neurofibres, the Agence Nationale de la Recherche through the Labex projects CSC (ANR-10-LABX-0026 CSC) and NIE (ANR-11-LABX-0058 NIE) within the Investissement d'Avenir program (ANR-10-120 IDEX-0002-02), the International Center for Frontier Research in Chemistry (icFRC), EPSRC Grants EP/K01711X/1, EP/K017144/1, EP/N010345/1, EP/L016057/1, and the Faraday Institution. The HAADF-STEM characterization was carried out in the Advanced Microscopy Laboratory (Dublin), a Science Foundation Ireland (SFI) supported centre.

Author contributions

S.I. and P.S. conceived the experiments and designed the study. A.G.K., Z.B., L.L., Y.A.S., A.C.F. and J.N.C. produced the raw materials and characterized them by spectroscopic and electrochemical techniques. S.I. designed and performed the multiscale characterizations on the final functionalized materials. R.F.O and M.A.S. designed and performed the charge carrier transport measurements and studies. D.I. carried out the NMR measurements and analysis. A.R., C.D. and V.N. designed and performed the HAADF-STEM investigations. All authors discussed the results and contributed to the interpretation of data. S.I., R.F.O, and P.S. co-wrote the paper with input from all co-authors.

ORCID

Stefano Ippolito: 0000-0002-6906-3961

Adam G. Kelly: 0000-0002-6070-7070

Rafael Furlan de Oliveira: 0000-0001-8980-3587

Marc-Antoine Stoeckel: 0000-0002-6410-4058

Daniel Iglesias: 0000-0002-1998-0518

Ahin Roy: 0000-0002-9515-2562

Clive Downing: 0000-0002-9209-0036

Zan Bian: 0000-0002-1659-8460

Lucia Lombardi: 0000-0002-6438-2971

Yarjan Abdul Samad: 0000-0001-9323-4807

Valeria Nicolosi: 0000-0002-7637-4813

Andrea C. Ferrari: 0000-0003-0907-9993

Jonathan N. Coleman: 0000-0001-9659-9721

Paolo Samorì: 0000-0001-6256-8281

Competing financial interests

The authors declare no competing financial interests.

Additional information

Supplementary information is available in the online version of the paper. Reprints and permission information is available online at www.nature.com/reprints. Correspondence and requests for materials should be addressed to P.S.